

Optical measurements of paired luminous rings in capacitive radio-frequency hydrogen discharges

Y. Sakawa,* M. Hori,† T. Shoji, and T. Sato‡

Department of Energy Engineering and Science, Nagoya University, Nagoya 464-8603, Japan

(Received 11 March 1999)

Optical measurements of paired luminous rings separated by a narrow dark gap have been conducted in capacitive radio-frequency (rf) hydrogen discharges. The lines of molecular H_2 are strongly excited at the ring emission compared with a weaker emission of the H_α line. The number of ring pairs increases with gas pressure, and the outermost ring pairs near the electrodes start to appear earlier than the inner ones. Each ring emission is turning on and off with the applied rf frequency, i.e., the left-side (right-side) ring of a paired ring is on when the left-side (right-side) electrode is biased positively. The axial light intensity profile, which is time resolved with the applied rf frequency, indicates that the emission profiles are similar to those of dc glow discharges, and the luminous rings correspond to the standing striations at the positive column.

[S1063-651X(99)12911-8]

PACS number(s): 52.80.Pi, 52.80.Hc

I. INTRODUCTION

Studies of moving and standing striations in positive columns started already in the last century. Research on striations up to 1968 were reviewed by Nedospasov [1], Pekarek [2], and Oleson and Cooper [3]. In the reviews, standing striations were covered briefly compared with detailed descriptions of the moving striations [1–3]. In 1980, Landa *et al.* reviewed experimental and theoretical studies of moving and standing striations [4]. However, most of the research is focused on dc discharges. Striations and Plasmoids in capacitive radio-frequency (rf) and audio-frequency (af) discharges, on the other hand, are rarely treated either experimentally [5–10] or theoretically [11,12], and are very poorly understood. Grous *et al.* studied the formation of striations in the positive column of an af (2–10 kHz) glow discharge using Ar and O_2 gases, and measured the number of striations as a function of the distance between the electrodes [10]. Schneider and Handel observed pairs of luminous disks separated by a dark gap in an rf discharge in H_2 and D_2 [13], which was interpreted as a plasma caviton induced by a resonance between an applied rf field and an ion oscillation [13, 14]. In most of the early experiments, however, time evolution and the time resolved measurements of the structure of the striations were not studied.

In this paper, we show detailed experimental investigation of the optical measurements of paired luminous rings observed in pulsed capacitive rf discharges with H_2 gas [15]. The experimental apparatus and parameters are similar to those in Ref. [13] except that the rf is applied with a pulse. The ring shaped structure of the emission is formed because the electrodes are surrounding the discharge tube. Paired

rings are clearly observed when H_2 or D_2 is used. The measured results indicate that the generation mechanism of the paired rings is similar to that of the standing striations in dc glow discharges.

This paper is organized as follows: Sec. II describes the experimental apparatus; in Sec. III the experimental results for H_2 are given; the model explaining the experimental results is discussed in Sec. IV; Sec. V presents the conclusion and a summary of the paper.

II. EXPERIMENTAL APPARATUS

Plasmas are created by a capacitive rf discharge as shown in Fig. 1. The electrodes are made of copper and are surrounding a Pyrex discharge tube of 85 mm in inner diameter and 500 mm in length. The electrode width $w = 60$ –100 mm and the electrode separation $d = 10$ –70 mm. A pulse modulated rf voltage (typical rf frequency $f = 1.2$ –1.5 MHz, zero to peak rf voltage $V_{rf} = 0.5$ –1.7 kV, rf power ≤ 1 kW, pulse length τ is typically 150 μ s, and repetition time t_r is typically 7 ms) is applied to the electrodes. A balanced matching circuit is used to allow symmetry of two output voltages with respect to the ground. In order to achieve better optical measurements in the radial direction, we placed a Pyrex tube of 40 mm in the outer diameter

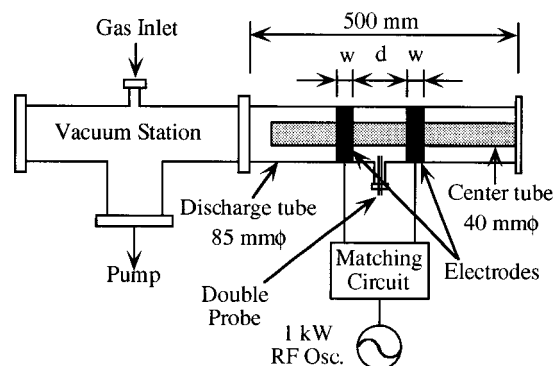


FIG. 1. Schematic view of the experimental setup.

*Electronic address: g44210a@nucc.cc.nagoya-u.ac.jp

†Present address: Fujitsu Ltd., 1-9-3 Nakase, Mihama-ku, Chiba 261, Japan.

‡Present address: Department of Electrical and Electronic Engineering, Iwate University, 4-3-5 Ueda, Morioka 020, Japan.

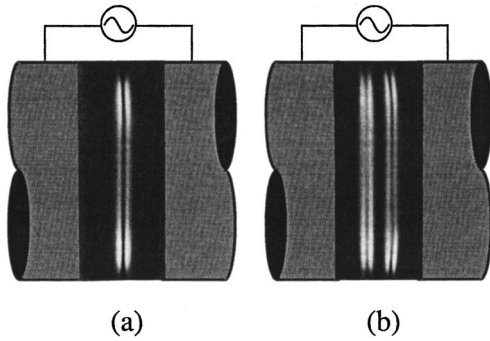


FIG. 2. Photographs of (a) one and (b) two pairs of rings at $P_1=1.71$ Torr and $P_2=1.92$ Torr, respectively. $V_{\text{rf}}=1.0$ kV, $f=1.5$ MHz, $d=3$ cm, $w=10$ cm, $\tau=150$ μs , and $t_r=7$ ms. Typical dimensions of the rings as measured by a scanning diode-array camera (SDAC), are the width of each ring ≈ 1 mm, the outer diameter ≈ 80 mm, the inner diameter ≈ 50 mm, and the dark-gap width ≈ 2 mm.

concentric with the discharge tube (vacuum region is at $r=20$ – 42.5 mm). A sheet of black paper was inserted inside the center tube to prevent emissions from the other side of the luminous rings from coming into view. The paired emissions are in a ring shape even without the center tube. It is confirmed that the center tube does not affect the generation of the ring emissions. The base pressure is ≈ 10 mTorr. The experiments were conducted with H_2 at a pressure range of $P < 5$ Torr.

III. EXPERIMENTAL RESULTS

When the H_2 pressure P is increased up to a critical pressure P_1 , a pair of luminous rings separated by a narrow dark gap is produced in the middle of the two electrodes. Two pairs of rings are abruptly produced by increasing P up to the next critical value P_2 . Photographs of one and two paired rings at P_1 and P_2 are shown in Figs. 2(a) and 2(b), respectively. The rings are axially symmetric with respect to the midplane of two electrodes and produced only in pairs.

The ring shaped emission from the plasma is formed because the annular electrodes surround the Pyrex discharge tube. However, when d is large, roughly $d > 70$ mm, the shape of the emission becomes a disk as was observed in Ref. [13].

The plasma density [$n_p \approx 10^9$ –(5×10^{10} cm^{-3})] and the electron temperature ($T_e \approx 2.5$ eV) are measured by a radially movable double probe. The axial profiles of n_p and T_e are measured by moving the electrodes in the axial direction. In the axial direction, n_p has maxima near the electrodes and a minimum at the midplane between the electrodes.

A. Time and spectrally resolved emission profile

Time and spectrally resolved emission profiles are measured as follows: The light emitted in the radial direction is focused by a $f/30$ lens to an entrance slit of an optical fiber (0.1 mm wide and 10 mm long). Both are placed on an axially movable stage located roughly 20 mm from the discharge tube. The optical fiber leads to a 250-mm focal length monochromator (1200 lines/mm, blazed for 500 nm, and spectral resolution=0.3–4.5 nm). A photomultiplier tube is

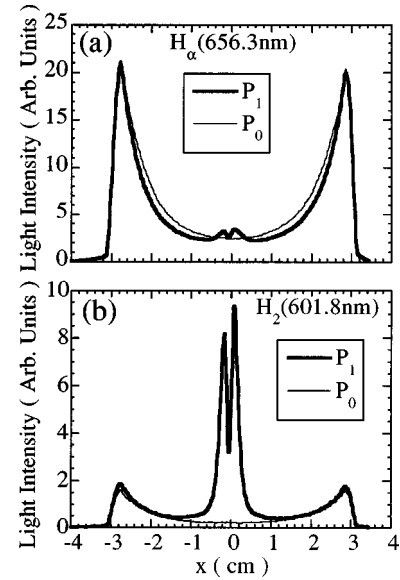


FIG. 3. Axial profiles of spectral intensity of (a) H_α and (b) H_2 (601.8 nm: $d^3\Pi_u; v'=0 \rightarrow a^3\Sigma_g^+; v'=0$). $V_{\text{rf}}=1.0$ kV, $P_0=1.08$ Torr, $P_1=1.47$ Torr, $f=1.2$ MHz, $d=6$ cm, $w=3$ cm, $\tau=250$ μs , and $t_r=7$ ms.

connected to the exit slit of the monochromator, and the converted signal is time resolved by a boxcar integrator.

The measured spectra of the ring emissions show that when no ring pairs appear (gas pressure P_0), lines from the H atoms [H_α (656.3 nm) and H_β (486.1 nm)] are dominant. When ring pairs appear at $P \geq P_1$, lines from the H_2 molecules, in addition to H_α and H_β , are strongly emitted from the rings. Figure 3 shows the axial light intensity profiles of H_α [Fig. 3(a)] and H_2 (601.8 nm) [Fig. 3(b)], which is the strongest emission among the lines of H_2 molecules, measured at P_0 and P_1 . When a pair of rings appears at P_1 , compared to only a slight increase in H_α , H_2 light intensity increases more than an order of magnitude. The 601.8 nm emission is representative of an electron excitation behavior in H_2 discharges [16]. The electron energies at which the excitation cross sections for H_2 and H_α become maximum are ≈ 16 eV [17] and ≈ 80 eV [18], respectively. Therefore, the energy of the electrons that causes the strong emission of H_2 light from the rings might be lower than the energy of those that causes the emission near the electrodes.

P dependence of H_2 (601.8 nm) light intensity profile is shown in Fig. 4. At P_0 [Fig. 4(a)], when P is increased from 0.15 to 1.08 Torr, the decay length of the light intensity, which peaks in the vicinity of the electrodes, becomes smaller. A pair of luminous rings is generated at $x \approx 0$ at P_1 [Fig. 4(b)]. The number of the ring pairs increases with P . Figures 4(c) and 4(d) show H_2 light intensity at P_5 and P_9 , respectively. Note that the distance between the neighboring ring pairs and the dark-gap width are nearly the same for all pairs.

Figure 5 shows time evolution of the axial profile of the zeroth-order light (total light) from the monochromator measured with $\tau=5$ ms and $t_r=50$ ms at P_5 (the pressure that five ring pairs exist at the typical experimental condition of $\tau=150$ μs and $t_r=7$ ms). As shown in Fig. 5(a), no ring pairs exist early in time. Two pairs of rings which are closest to the electrodes ($x = \pm 1$ cm) start to appear at $t \approx 80$ μs

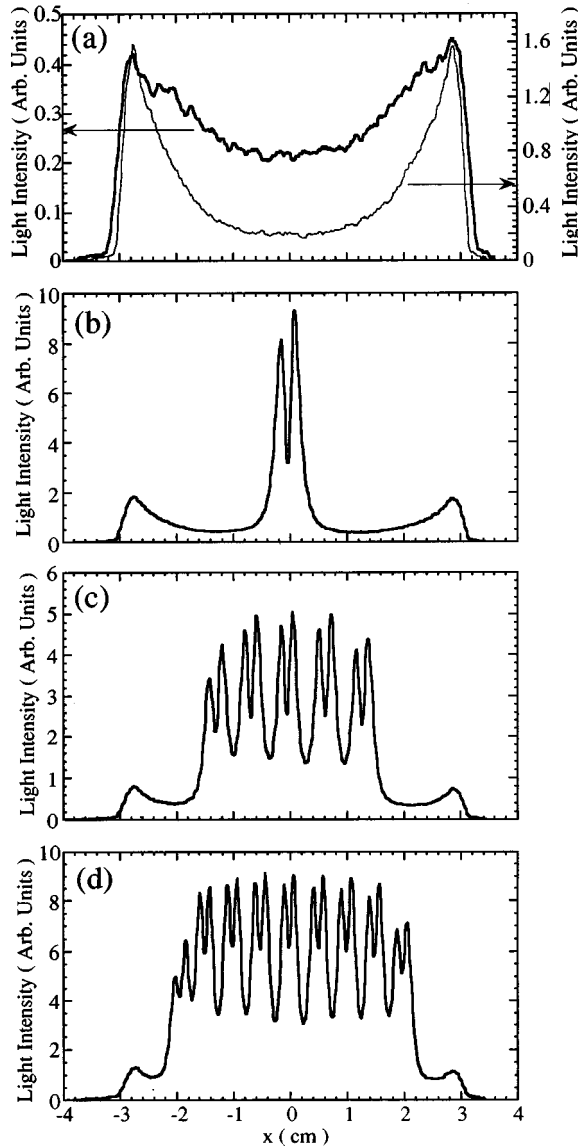


FIG. 4. H₂ pressure dependence of the axial profiles of spectral intensity of H₂ (601.8 nm). (a) $P_0 = 0.15$ Torr (thick line) and 1.08 Torr (thin line), (b) $P_1 = 1.47$ Torr, (c) $P_5 = 2.06$ Torr, and (d) $P_9 = 2.61$ Torr. $V_{rf} = 1.0$ kV, $f = 1.2$ MHz, $d = 6$ cm, $w = 3$ cm, $\tau = 250$ μ s, and $t_r = 7$ ms.

[Fig. 5(b)]. The inner ring pairs at $x \approx \pm 0.5$ cm and that at $x = 0$ appear at $t \approx 90$ μ s [Fig. 5(c)] and 100 μ s [Fig. 5(d)], respectively. The intensity of five pairs of rings keeps growing until $t \approx 170$ μ s [Fig. 5(e)] and remains nearly constant until $t \approx 300$ μ s. The position of the rings starts to move towards the negative x direction at $t > 300$ μ s. At the same time, the intensity of the far left ring pairs decreases and finally disappears [Figs. 5(f) and 5(g)]. At $t \geq 2000$ μ s, the intensity and structure of the remaining three ring pairs are unchanged until the end of the rf pulse [Fig. 5(h)]. We call the sequences $t \leq 170$ μ s, $t = 170 - 300$ μ s, $t = 300 - 2000$ μ s, and $t \geq 2000$ μ s the growing state (GS), the quasistable state (QSS), the decaying state (DS), and the steady state (SS), respectively. Note that at GS and QSS, the positions of the luminous rings are nearly unchanged. The structures at SS are different from those at QSS. For example, when 20 pairs of rings exist at QSS, the number decreases to 13 at SS. We

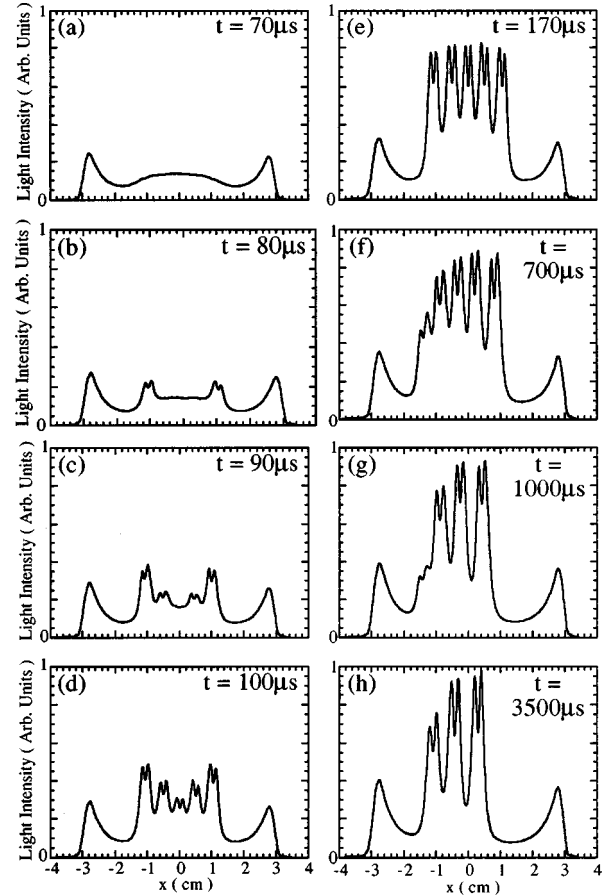


FIG. 5. Time evolution of the axial profiles of the total light intensity at $P_5 = 2.49$ Torr. $V_{rf} = 1.0$ kV, $f = 1.2$ MHz, $d = 6$ cm, $w = 3$ cm, $\tau = 5$ ms, and $t_r = 50$ ms. $V_{rf}(t)$ is applied to the electrodes at $t = 0$, and the gate width of the boxcar integrator is 10 μ s.

believe that the structure at SS is the one which Schneider and Handel observed in cw discharges [13]. In this paper, we focus on the phenomena at GS and QSS to investigate the evolution of the paired rings. Therefore, most of the measurements were conducted at the pulse length $\tau < 300$ μ s.

A detailed time evolution of the axial profile of H₂ (601.8 nm) light intensity at P_0 at GS and QSS is shown in Fig. 6. We see that the emission at $|x| < 2$ cm is larger than that near the electrodes at $t = 5$ μ s [Fig. 6(a)]. The emission at $x = 0$ decreases nearly an order of magnitude at QSS ($t = 100$ μ s) [Fig. 6(f)], while, that near the electrodes slightly increases. At $t = 50 - 70$ μ s, a dip exists at $x = 0$ [Fig. 6(d)], however, it disappears at QSS. Figure 7 shows the time evolution of the axial profile of H₂ (601.8 nm) light intensity at P_1 . The emission profiles at $t \leq 40$ μ s are similar to the ones shown in Figs. 6(a)–6(c). A dip (dark gap) at $x = 0$ is not formed yet at $t = 74$ μ s [Fig. 7(a)]. Once a dip appears at $t = 82$ μ s [Fig. 7(b)], the ring emission starts growing [Fig. 7(c)], and the light intensity increases nearly an order of magnitude at QSS ($t = 120$ μ s) [Fig. 7(d)]. Time evolution of the axial profile of H₂ (601.8 nm) light intensity at P_2 is shown in Fig. 8. The emission profiles at $t \leq 40$ μ s are similar to those shown in Figs. 6(a)–6(c). Note that two dark gaps at $x \approx \pm 0.5$ cm appear simultaneously at $t \approx 60$ μ s [Fig. 8(a)] before the light intensity at $x = 0$ starts to decrease at $t \approx 70$ μ s [Fig. 8(d)]. From these results, it seems that the strong emissions from

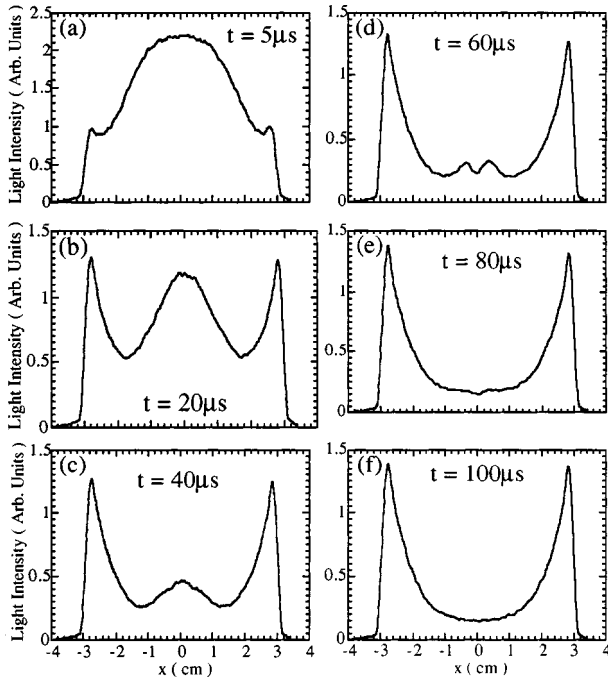


FIG. 6. Time evolution of the axial profiles of H_2 (601.8 nm), light intensity at $P_0=1.33$ Torr. $V_{rf}=1.0$ kV, $f=1.2$ MHz, $d=6$ cm, $w=3$ cm, $\tau=200$ μ s, and $t_r=4$ ms.

the paired rings are excited after the dark gaps (dark regions between a pair of rings) are formed.

Now we show the results of the optical measurements of the paired rings which are time resolved with the period of the applied rf. Time variations of H_2 (601.8 nm) light intensity for the left- and the right-side rings from a pair of rings separated by a dark gap measured at QSS are shown in Fig. 9(a). The instantaneous voltage $V_{rf}(t)$ applied to the left-side electrode is also shown in the figure. We see that both rings turn on and off at the rf frequency of 1.2 MHz (0.83 μ s). Furthermore, the left-side ring is on when $V_{rf}(t)$ applied to the left-side electrode is positive, while the right-side ring is on when $V_{rf}(t)$ applied to the left-side electrode is negative. Figures 9(b), 9(c), and 9(d) show the axial light intensity

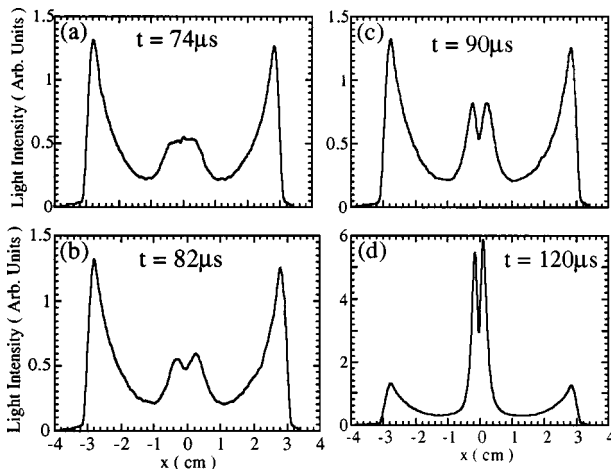


FIG. 7. Time evolution of the axial profiles of H_2 (601.8 nm) light intensity at $P_1=1.47$ Torr. $V_{rf}=1.0$ kV, $f=1.2$ MHz, $d=6$ cm, $w=3$ cm, $\tau=200$ μ s, and $t_r=4$ ms.

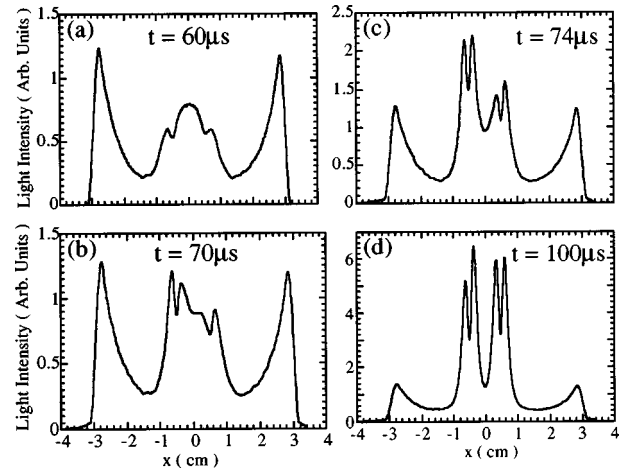


FIG. 8. Time evolution of the axial profiles of H_2 (601.8 nm) light intensity at $P_2=1.57$ Torr. $V_{rf}=1.0$ kV, $f=1.2$ MHz, $d=6$ cm, $w=3$ cm, $\tau=200$ μ s, and $t_r=4$ ms.

profiles of H_α and H_2 lines at P_1 , and the H_2 line at P_5 , respectively, when the left- and the right-side ring emissions are maximum. From these results, it seems that the ring emissions are not excited by the electrons coming directly from the electrode regions, but by those at the dark gap between the paired rings. When $V_{rf}(t)$ applied to the left electrode is negative, an exponentially decaying emission peaked near the left electrode ($x=-2.8$ cm), multiple emissions from the right-side rings [Fig. 9(d)], and the weaker emission peaked near the right electrode ($x=+2.8$ cm) turn on. These emission profiles are quite similar to those of dc glow discharges, and each profile corresponds to the negative glow (NG), striations at the positive column (PC), and the anode glow, respectively [19]. Similar profiles are also observed in rf discharges without striations [19].

Figures 10(a) and 10(b) show the time variation of $V_{rf}(t)$ applied to the left-side electrode and H_2 (601.8 nm) light intensity of the right-side ring of a pair of rings separated by a dark-gap measured at P_1 , respectively. The light intensity grows quickly within a few cycles of rf then decreases nearly an order of magnitude before a pair of rings appears at $t \approx 95$ μ s [Fig. 10(b)]. At $t < 20$ μ s the emission at the central region is large, and the light intensity peaks both at the positive and negative peaks of $V_{rf}(t)$ [Fig. 10(c)]. This means that the emission at the central region before the ring pairs appear [see Figs. 6(a) and 6(b)] is excited by the electrons coming from both sides of the electrodes. Once the strong ring emission is excited at $t \approx 95$ μ s, the light intensity at the right-side ring is peaked only when the left-side electrode is negatively biased, as is shown in Figs. 10(d), 10(e), and 9(a). On the other hand, the light intensity measured in the vicinity of the right-side electrode ($x \approx 2.9$ cm) always peaks when the left-side electrode is positively biased (not shown).

B. Emission profile at QSS

By limiting τ less than time that DS starts, we can measure time integrated emission at QSS. P dependence of the ring position x observed by the scanning diode-array camera (SDAC) is shown in Fig. 11(a). The appearance of the n th pair of rings at critical pressures P_n ($n=1,2,\dots,9$) is clearly seen. At the pressure just before the transition from

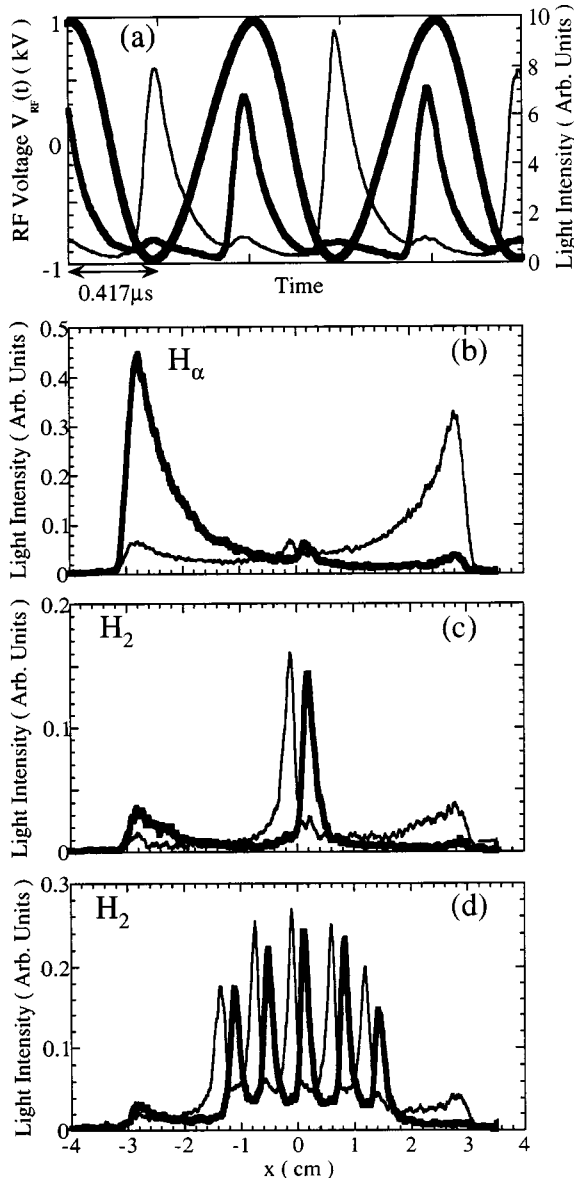


FIG. 9. (a) Time variations of H_2 (601.8 nm) light intensity of the left-side ring (thick line) and the right-side ring (thin line) of a pair of rings separated by a dark gap measured at $t = 200 \mu\text{s}$. $V_{rf}(t)$ applied to the left-side electrode is also shown in the figure ($V_{rf} = 1.0$ kV and $f = 1.2$ MHz). (b) H_α , (c) H_2 (601.8 nm) emission profiles at $P_1 = 1.37$ Torr, and (d) H_2 (601.8 nm) emission profiles at $P_5 = 1.95$ Torr, measured at the left-side emission is maximum (thin line) and the right-side emission is maximum (thick line). The gate width and the time delay of the boxcar integrator is 0.1 and 200 μs , respectively. $d = 6$ cm, $w = 3$ cm, $\tau = 250 \mu\text{s}$, and $t_r = 5$ ms.

one to two ring pairs occurs, the position of a ring pair shifts ≈ 1 mm towards positive x direction. A slight increase in P causes a sudden appearance of two ring pairs at $x \approx \pm 2.5$ mm. By increasing P , the position of two ring pairs moves outward, and the distance between two ring pairs becomes wider. At $P = P_3$, the third ring pair appears at $x \approx 0$. We define the distance from an inner edge of the electrode ($x = \pm 15$ mm) to the dark gap of the outermost ring pair as L , the distance between the outermost ring pair and the neighboring pair as l , and the dark gap width as Δ [see Fig. 11(a)]. P dependence of L and l [Fig. 11(b)], and Δ [Fig.

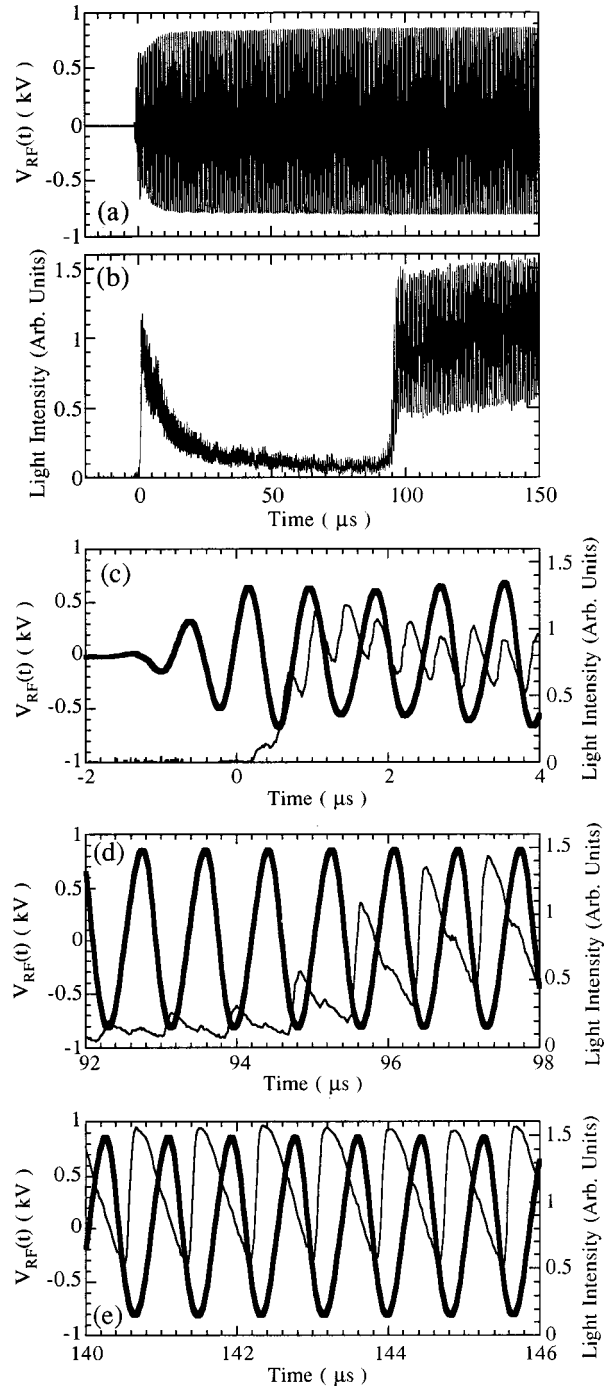


FIG. 10. Time variation of (a) $V_{rf}(t)$ applied to the left-side electrode and (b) H_2 (601.8 nm) light intensity of the right-side ring of a pair of rings separated by a dark gap. (c), (d), and (e) are the expanded $V_{rf}(t)$ (thick line) and H_2 light intensity (thin line). $P_1 = 1.47$ Torr, $d = w = 3$ cm, and $f = 1.2$ MHz.

11(c)], are reduced from Fig. 11(a). Even though the appearance of the n th pair of rings at P_n is abrupt, both L and l vary smoothly with P , which scale as $L \propto P^{-2.6}$ and $l \propto P^{-1.5}$. Δ slightly decreases with P , i.e., decreases when the number of ring pairs increases. Even at P_9 the variation in Δ among nine ring pairs is the same within 0.4 mm.

Figure 12(a) shows V_{rf} dependence of the ring position x . By decreasing V_{rf} , the number of ring pairs increases from four to six, and no discharge occurs at $V_{rf} < 0.55$ kV. V_{rf}

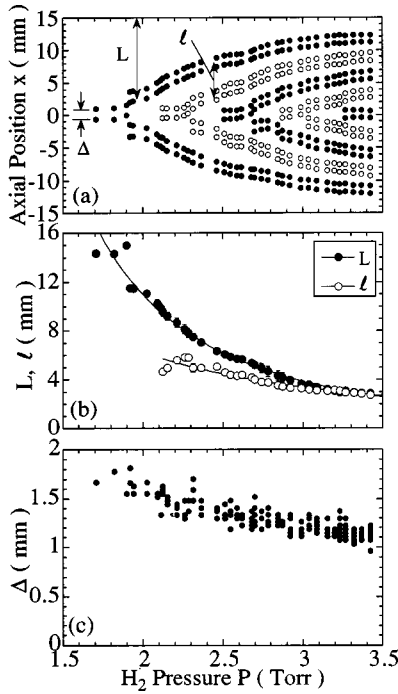


FIG. 11. (a) H_2 pressure (P) dependence of the ring position (x) observed by the SDAC. Different marks (open and closed circles) are used for convenience. The pressure dependence of (b) L , l and (c) Δ reduced from (a). The solid lines in (b) represent fits to L , $l \propto P^{-m}$ dependence. m is 2.6 and 1.5 for L and l , respectively. $V_{rf} = 1.0$ kV, $f = 1.5$ MHz, $d = 3$ cm, $w = 10$ cm, $\tau = 150 \mu\text{s}$, and $t_r = 7$ ms.

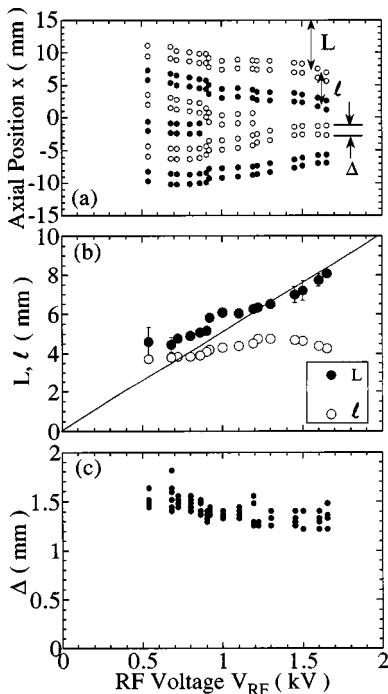


FIG. 12. (a) The rf voltage (V_{rf}) dependence of the ring position (x) observed by the SDAC. (b) V_{rf} dependence of L and l reduced from (a). $P = 2.55$ Torr, $f = 1.5$ MHz, $d = w = 3$ cm, $\tau = 150 \mu\text{s}$, and $t_r = 7$ ms.

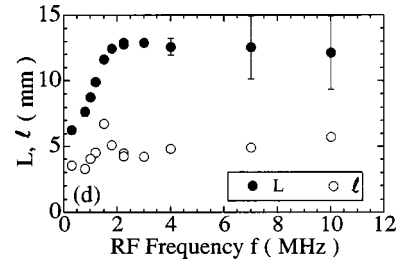


FIG. 13. The rf frequency (f) dependence of L and l . $P = 2.19$ Torr, $V_{rf} = 1.5$ kV, $d = w = 3$ cm, $\tau = 150 \mu\text{s}$, and $t_r = 7$ ms.

dependence of L and l , and Δ reduced from Fig. 12(a) are shown in Figs. 12(b) and 12(c), respectively. We see that L is roughly proportional to V_{rf} , while l shows weak V_{rf} dependence. Δ decreases with V_{rf} or increases with the number of ring pairs, which is different from the P dependence.

The frequency f dependence of L and l are shown in Fig. 13. Even though L increases by a factor of 2 when f is varied from 0.3 to 1.8 MHz (by a factor of 6), both L and l show nearly no f dependence at $f = 1.8 - 10$ MHz.

Figures 14(a) and 14(b) show d dependence of the position of the dark gaps (not the position of the luminous rings) [Fig. 14(a)] and the reduced L and l [Fig. 14(b)], respectively. We see that both L and l have no d dependence at $d \geq 30$ mm. No variations of L on d indicates that the ring pairs closest to the electrodes are “sticking” to the electrodes. Similar phenomena are observed in dc glow discharges, i.e., when the tube length is increased only the length of the PC becomes longer, while no variations are seen in cathode layers [20].

The electrode width w dependence of the position of the dark gap x [Fig. 15(a)] and the reduced L and l [Fig. 15(b)] are shown in Fig. 15. By increasing w from 0.5 to 16 cm, the number of ring pairs increases from one to nine. We see that L strongly depends on w , while l shows no w dependence.

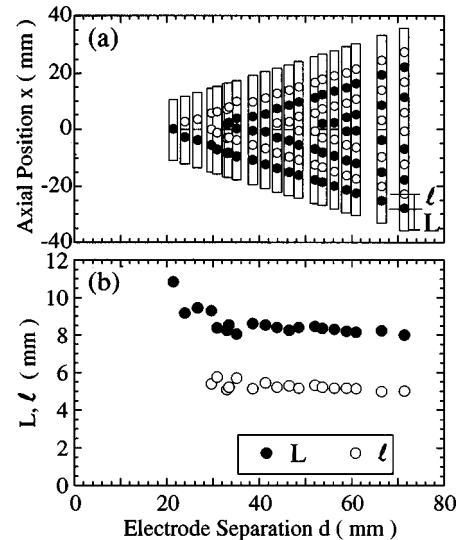


FIG. 14. (a) Electrode separation (d) dependence of the position of the dark gap (x). The position of two electrodes are also plotted. (b) Reduced d dependence of L (closed circle) and l (open circle) from (a). $P = 2.47$ Torr, $V_{rf} = 1.0$ kV, $f = 1.5$ MHz, $w = 10$ cm, $\tau = 300 \mu\text{s}$, and $t_r = 7.5$ ms.

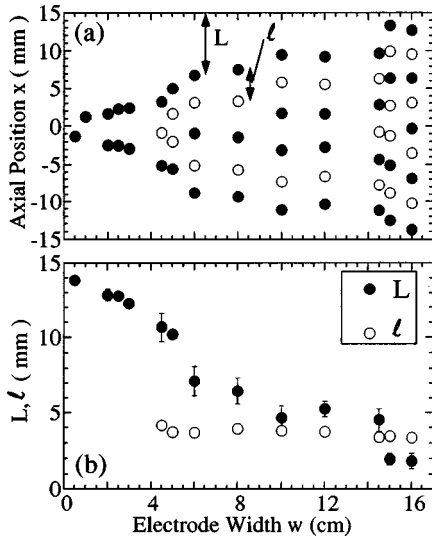


FIG. 15. (a) Electrode width (w) dependence of the position of the dark gap (x). (b) Reduced w dependence of L (closed circle) and l (open circle) from (a). $V_{\text{rf}}=0.7$ kV, $P=2.7$ Torr, $f=1.5$ MHz, $d=3$ cm, $\tau=150\text{--}600$ μs , and $t_r=7$ ms.

IV. DISCUSSION

The experimental findings can be summarized as follows: (a) The strong emission from the paired luminous rings is excited by slow electrons. (b) The paired rings appear from the pairs closest to the electrodes. (c) The dark gap appears first, then ring pairs are excited at both sides of the dark gap. (d) The left- and right-side rings turn on and off with the applied rf frequency; the left-side (right-side) ring is on when $V_{\text{rf}}(t)$ applied to the left-side electrode is positive (negative). (e) L and l have $L \propto V_{\text{rf}}/P^{2.6}$ and $l \propto 1/P^{1.5}$ dependence, respectively, but no f ($f=1.8\text{--}10$ MHz) and d ($d \geq 30$ mm) dependence. Furthermore, l does not depend on w , while L does.

In dc glow discharges, the pressure dependence of l is expressed by Goldstein's law $l \propto P^{-m}$, where $m=0.53$ for H_2 [21]. The pressure dependence of l in rf discharges has been measured, to the best of our knowledge, only for Ar, which shows $m=0.16$ [5]. Our measured results of $m=1.5$ for H_2 is different from those of dc glow discharges. The measured luminous ring pairs look, at a first glance, similar to double striations observed in dc discharges [22]. However, as shown in Figs. 9(b)–9(d), by time resolving the emission with the time scale of the rf, only one ring of a ring pair is on, i.e., both rings of a set of paired rings never turn on simultaneously. Therefore, the measured luminous ring pairs are different from double striations. When the emission is time resolved with the period of the applied rf, it shows the axial profile similar to that in dc glow discharges, i.e., the NG, the PC with or without standing striations, and the anode glow. From these results, we believe that the theory to explain the generation mechanism of standing striations in dc glow discharges is basically applicable to paired luminous rings in rf discharges if the phenomena are time resolved with the period of the applied rf.

In dc glow discharges it is proposed that if the Faraday dark space (FDS) length L_{FDS} exceeds the energy relaxation length λ_T of untrapped intermediate energy electrons, i.e., $L_{\text{FDS}} > \lambda_T$, the ionization process is localized in the transi-

tion region from the FDS to the PC [23]. This is because a second field reversal exists at the end of the FDS in order to compensate for electron diffusion towards the anode, and the electron kinetic energy at the field reversal is much less than the excitation or the ionization energy. The localization of the ionization source may produce self-maintained spatially periodic potential profiles and the electron distribution function (EDF) and may cause standing striations [23]. These potential profiles and EDF are observed in H_2 glow discharges, i.e., a periodic staircase potential with potential steps of ≈ 10 V at the position of striations and a group of high-energy primary electrons with a mean energy ≈ 10 eV larger than that of low-energy bulk electrons are observed [24]. Electrons are accelerated at the potential step and excite striations. $L_{\text{FDS}} > \lambda_T$ is satisfied in our experiments since $\lambda_T < 0.3$ cm for $P > 1.5$ Torr, and this model might be applicable. We believe that at the condition when the ring emission is excited in our experiment, staircase axial potential profile is formed in the half-period of the rf, i.e., the potential increases stepwise from the cathode side of the electrode to that of the anode side, and the positions of the potential jumps correspond to those of the ring emissions. Electron and ion rich potentials are formed at the cathode and anode sides of the potential jump, respectively.

Now we pay attention to GS ($t < 170$ μs in Fig. 5), especially to the time period between $t=80$ μs (T_1) and 90 μs (T_1+T_2), at which only outermost ring pairs at $x \approx -1$ and $+1$ cm are excited as shown in Fig. 5(b). Note that even at this period, the left- and right-side rings both at $x \approx -1$ and $+1$ cm are turning on and off with the period of the applied rf ($T_{\text{rf}}=1/f=0.83$ μs). This alternate emission occurs such that when the left-side (right-side) electrode is biased positively, only the left-side (right-side) rings both at $x \approx -1$ and $+1$ cm are turning on. From these results, we believe that T_1 is the time required to create potential steps only at the dark gaps of the outermost ring pairs, and that luminous rings are excited by those electrons which are accelerated by the potential steps. Furthermore, it seems that the position of the potential steps does not move but just changes the direction of the rf electric field with T_{rf} . Because of the axial symmetry of the discharge with respect to the midplane of the two electrodes, the potential step at the dark gap at $x \approx -1$ cm ($x \approx +1$ cm) might be created when the left-side electrode is biased negatively (positively). This axial motion of the electrons might be caused by the rf electric field which changes its direction every half-cycle of the rf.

The model to explain the generation of luminous rings is based on the energy relaxation of slower electrons resulting from inelastic collision as described in Ref. [23]: Some electrons are accelerated from the second field reversal, which is located at the boundary between the FDS and the PC, and lose their kinetic energy by inelastic collision when they move a length of acquisition of the lowest excitation energy (λ_e). The position of the first potential step or the standing striation from the cathode is determined by the length λ_e from the second field reversal. In our experiments, therefore, the distance from the electrode to the outermost ring pairs L might be expressed by (length of the NG)+(length of the FDS)+ λ_e .

Now we consider the generation mechanism of the inner

rings. It seems that potential differences that are not large enough to cause localized ionization are formed at $x \approx -0.5, 0,$ and $+0.5$ cm at $t \approx T_1$ [Fig. 5(b)]. After the staircase potentials with large enough potential steps are formed at the outermost dark gaps, it takes about T_2 to create other potential steps at the inner dark gaps at $x \approx +0.5$ cm [Fig. 5(c)]. The axial motion of the electrons from the outermost ring to the inner ring might also be caused by the rf electric field, i.e., the electrons which lose almost all the kinetic energies at the end of the potential steps of the outermost dark gaps move inward to the anode side due to the rf electric field. The longer generation time of the outermost ring pairs ($T_1 = 80 \mu\text{s}$) compared with that of the inner rings ($T_2 = 10 \mu\text{s}$) might be caused by the time required to build up the plasma after the rf is turned on at $t=0$. The distance from the outermost ring pairs to the inner rings l might be decided by λ_e . In order to explain the measured dependence of L and l on P and V_{rf} , the detailed measurement of the axial electric field is necessary.

As described in the model, the ring emission is excited by the slow electrons which are accelerated by the potential steps, which might be of the order of 10 V. Therefore, the emission of H_2 lines is strongly excited compared with H_α emission at the ring (Fig. 3). When the ring emissions are excited at $P \geq P_1$, the electrons coming from the left-side (right-side) electrode create the potential steps at $x < 0$ ($x > 0$) because of the axial symmetry as mentioned above. By decreasing P , L increases with $L \propto P^{-2.6}$ (Fig. 11), i.e., the distance between the electrode and the outermost potential step becomes longer. At P_2 (see Fig. 8), the potential step is created at $x = \pm 0.5$ cm, where the dark gap appears. Once the potential step is formed the electrons excite the ring pairs at both sides of the dark gap. At P_1 (see Fig. 7), the electrons from both electrodes create the potential step at $x=0$, i.e., at $L = d/2$. By decreasing P further, L is now longer than $d/2$ at P_0 (see Fig. 6), and a potential step formed in the first half-cycle of the rf by the electrons from one side of the electrodes may be smeared out in the other half-cycle by the electrons from the other side of the electrodes. As a result, the potential step is not formed, and no ring pairs appear at P_0 .

V. CONCLUSIONS

In conclusion, optical measurements of paired luminous rings separated by a narrow dark gap have been conducted in pulsed capacitive rf hydrogen discharges. The evolution of the luminous rings is divided into four states, i.e., GS, QSS, DS, and SS. The positions of ring pairs are nearly unchanged at GS and QSS. Therefore, time and spectrally resolved emission profiles have been measured at GS and QSS. The experimental findings can be summarized as follows: (a) The ring shaped structure of the emission is formed because a pair of electrodes are surrounding the Pyrex discharge tube. (b) The strong emission from the paired luminous rings is excited by slow electrons. As a result, the lines of molecular H_2 are strongly excited at the ring emission compared with a weaker emission of H_α line. (c) The outermost ring pairs near the electrodes start to appear earlier than the inner ones. The dark gap appears first, then ring pairs are excited at both sides of the dark gap. (d) The left- and right-side rings turn on and off with the applied rf frequency, i.e., the left-side (right-side) ring is on when $V_{\text{rf}}(t)$ applied to the left-side electrode is positive (negative). (e) The axial light intensity profile, which is time resolved with the applied rf frequency, indicates that the emission profiles are similar to those of dc glow discharges, and the luminous rings correspond to the standing striations at the PC. (f) At QSS, L and l have $L \propto V_{\text{rf}}/P^{2.6}$ and $l \propto 1/P^{1.5}$ dependence, respectively, but no f ($f = 1.8 - 10$ MHz) and d ($d \geq 30$ mm) dependence. Therefore, the number of ring pairs increases with P and decreases with V_{rf} .

Finally, even though the physical mechanism creating the paired luminous rings in rf discharges seems to be similar to that of the standing striations in dc glow discharges, we have observed differences between the two. For example, the measured $l \propto P^{-1.5}$ dependence is different from the $l \propto P^{-0.53}$ dependence in dc glow discharges, and the existence of the GS, QSS, and DS in addition to SS is not predictable from the simple theory described here. Phenomena of spatially nonuniform structures in rf discharges are important in various fields of applied physics such as plasma assisted material processing. We believe that the observed phenomena are rich in the underlying physics and important for the understanding of the basic physics of striations.

-
- [1] A. V. Nedospasov, Usp. Fiz. Nauk **94**, 439 (1968) [Sov. Phys. Usp. **11**, 174 (1968)].
- [2] L. Pekarek, Usp. Fiz. Nauk **94**, 463 (1968) [Sov. Phys. Usp. **11**, 188 (1968)].
- [3] N. L. Oleson and A. W. Cooper, *Advances in Electronics and Electron Physics*, edited by L. Marton (Academic, New York, 1968), Vol. 24, p. 155.
- [4] P. S. Landa, N. A. Miskinova, and Yu. V. Ponomarev, Usp. Fiz. Nauk **132**, 601 (1980) [Sov. Phys. Usp. **23**, 813 (1980)].
- [5] A. A. Zaitsev and Kh. A. Dzherpetov, Zh. Eksp. Teor. Fiz. **24**, 516 (1953).
- [6] M. Klerk, in *Proceedings of the Fourth International Conference on Ionization Phenomena in Gases, 1959, Uppsala* (North-Holland, Amsterdam, 1960), Vol. I, p. 283.
- [7] A. J. Hatch, in *Proceedings of the Fourth International Conference on Ionization Phenomena in Gases, 1959, Uppsala* (Ref. [6]), Vol. I, p. 314.
- [8] A. J. Hatch, in *Proceedings of the Fifth International Conference on Ionization Phenomena in Gases, 1961, Munich* (North-Holland, Amsterdam, 1962), Vol. I, p. 748.
- [9] A. Miller, C. W. Bruce, and M. D. Kregel, J. Appl. Phys. **39**, 1853 (1968).
- [10] CS. Grosu, S. Talasman, F. Stamate, and M. Andreescu, in *Proceedings of the Thirteenth International Conference on Phenomena in Ionized Gases, 1977, Berlin* (Physical Society of the GDR, Berlin, 1977), Vol. I, p. 267.
- [11] Yu. R. Alanakyan and L. A. Mikhalev, Zh. Tekh. Fiz. **45**, 1809 (1975) [Sov. Phys. Tech. Phys. **20**, 1152 (1975)].
- [12] B. S. Kerner and V. V. Osipov, Radio Eng. Electron. Phys. **27**, 122 (1982); **28**, 119 (1983).
- [13] R. T. Schneider and P. H. Handel, Fusion Technol. **7**, 316 (1985).

- [14] P. H. Handel and R. T. Schneider, *Fusion Technol.* **7**, 320 (1985).
- [15] Y. Sakawa, M. Hori, T. Shoji, and T. Sato, *Phys. Plasmas* **5**, 1179 (1997).
- [16] C. Barbeau and J. Jolly, *J. Phys. D* **23**, 1168 (1990).
- [17] G. R. Möhlmann and F. J. de Heer, *Chem. Phys. Lett.* **43**, 240 (1976).
- [18] H. Tawara, Y. Itikawa, H. Nishimura, and M. Yoshino, *J. Phys. Chem. Ref. Data* **19**, 617 (1990).
- [19] Y. P. Raizer, *Gas Discharge Physics* (Springer-Verlag, Berlin, 1991).
- [20] J. J. Thomson and G. P. Thomson, *Conduction of Electricity Through Gases* (Dover, New York, 1932).
- [21] F. Wehner, *Ann. Phys. (Leipzig)* **32**, 49 (1910).
- [22] W. De La Rue and H. W. Muller, *Philos. Trans. R. Soc. London* **169**, 155 (1878); A. Güntherschulze and H. Meinhardt, *Z. Phys.* **110**, 95 (1938); M. J. Druyvesteyn and F. M. Penning, *Rev. Mod. Phys.* **12**, 87 (1940).
- [23] L. D. Tsendin, *Fiz. Plazmy* **8**, 400 (1982) [*Sov. J. Plasma Phys.* **8**, 228 (1982)]; V. I. Kolobov and L. D. Tsendin, *Phys. Rev. A* **46**, 7837 (1992); V. I. Kolobov and V. A. Godyak, *IEEE Trans. Plasma Phys.* **PS-23**, 503 (1995).
- [24] R. L. F. Boyd and N. D. Twiddy, *Proc. R. Soc. London, Ser. A* **259**, 145 (1960); N. D. Twiddy, *ibid.* **275**, 338 (1963).